Local atomic structure and the valence band structure of the rhombic-triacontahedral quasicrystal, its 1/1 approximant, and the Mackay-icosahedral quasicrystal in the Al-Mg-Pd alloy system

Tsunehiro Takeuchi, Uichiro Mizutani, Shinji Yamaguchi, Toshiharu Fukunaga, and Takayuki Mizuno
Department of Crystalline Materials Science, Nagoya University, Nagoya 464-8603, Japan

Nobuo Tanaka
Department of Applied Physics, Nagoya University, Nagoya 464-8603, Japan
(Received 10 November 1997; revised manuscript received 23 June 1998)

The rhombic-triacontahedral-type quasicrystal (RT-QC), its (1/1, 1/1, 1/1) approximant (RT-1/1) and the Mackay-icosahedral-type quasicrystal (MI-QC) can be formed in the Al-Mg-Pd system. The radial distribution function RDF(r) spectra of the three compounds is derived from neutron diffraction experiments. Powdered x-ray diffraction Rietveld refinement is also carried out to determine the atomic structure of the RT-1/1, and the refined data are converted to the RDF(r). The interatomic distance of the Al-Pd pair in the RT-1/1 and RT-QC is found to be remarkably shortened relative to that calculated from the hard sphere model with Goldschmidt radii. In the MI-QC, the interatomic distance of the Al-Pd pair is further shortened. In addition, the shortening of the interatomic distance is also observed in the Mg-Pd pair. The valence band spectra studied by the x-ray photoemission spectroscopy and soft x-ray spectroscopy clearly show the formation of the bonding and antibonding states associated with the Al-Pd and Mg-Pd atomic pairs in the MI-QC. The results are consistent with the shortening of the interatomic distances derived from the structure analysis. The reason for the possession of the highest resistivity in the MI-QC among the three compounds is attributed to the formation of the covalent bonding between Al-Pd and Mg-Pd atomic pairs. [S0163-1829(98)06841-6]

I. INTRODUCTION

Several highly ordered quasicrystals like Al-Cu-Ru and Al-Pd-Re show unusually high resistivities comparable to those of heavy doped semiconductors.[1–6] The Hall coefficients are known to change their sign with increasing temperature,[7] and their behavior is apparently dependent on sample preparation condition.[8] These unique transport properties have been discussed in relation to a marginally metallic alloy in the proximity to a metal-insulator transition. A number of investigations so far accumulated are apparently consistent with the conclusion that a highly ordered long-range quasiperiodicity yields the sharp multiply-fold Brillouin zones and the resulting deep pseudogap in the density of states at the Fermi level is responsible for the possession of low carrier densities. However, low density of states alone cannot account for a diversity of the transport behaviors observed in many different quasicrystals.

There are two different families in the icosahedral quasicrystals. Rhombic-triacontahedral-type quasicrystals (hereafter abbreviated to RT-QC's) are composed of only non-transition metal elements and exhibit ordinary metallic behavior similar to those observed in nonmagnetic amorphous alloys, even when they are characterized by a highly ordered quasiperiodicity with the pseudogap at E_F. In contrast, the Mackay-icosahedral quasicrystals (MI-QC's) involve the transition metal elements and exhibit resistivities much higher than those in the RT-QC's. Admittedly, the pseudogap of the RT-QC is generally slightly shallower than that of the MI-QC. However, a substantial difference in the electron transport properties between the RT-QC and MI-QC cannot be solely ascribed to the difference in the depth of the pseudogap.

Recently, we have studied the electronic structure of the RT-type and MI-type Al-Mg-Pd, RT-type Al-Mg-Zn and MI-type Al-Pd-Re quasicrystals by means of the x-ray photoemission spectroscopy (XPS), soft x-ray emission spectroscopy (SXES) and low temperature specific heat measurements.[9–11] A comparison of the valence band structures between the MI-QC's and the RT-QC's allowed us to conclude that the pseudogap formed near E_F in the MI-QC is always heavily influenced by the bonding and antibonding states arising from the hybridization between Al-3p electrons and d electrons of transition metals. A large number of analysis based on SXES and soft-x-ray absorption spectroscopy (SXAS) measurements here were made for other quasicrystals by Beline *et al.*,[12] and they have also found the hybridization effects between Al and transition metals as well as the pseudogap at E_F. Krajčí *et al.*[13] pointed out as a consequence of the theoretical calculation for a series of approximants that the hybridization between Al and transition metal elements is strong in the Al-Pd-Mn MI-QC, and that the hybridized states enhance the pseudogap at E_F. We believe that the formation of the pseudogap coupled with the antibonding states just below E_F must be responsible for the enhancement in the electrical resistivity of the MI-QC's.

The bonding states observed in the valance band must be reflected in the local atomic structure, especially the interatomic distance between the relevant atomic pair. In the present work, we have studied both the atomic and electronic structures of the MI-QC's and RT-QC's with particular attention to possible interrelationship of the local atomic structure, the electronic structure and the electron transport properties. We selected the Al-Mg-Pd alloy system for this particular purpose, since three different compounds including the RT-QC, its 1/1 approximant (hereafter abbreviated to RT-1/1) and the MI-QC can be obtained.

TABLE I. Electronic properties of the Al-Mg-Pd quasicrystals and their approximants. The data of the Al-Mg-Zn RT compounds are also listed. (Ref. 14) (a), (b), and (c) refer to the samples used for the structural analysis.

Phase		Composition	γ (mJ/mol K^2)	$\rho_{300\,K}$ ($\mu\Omega$ cm)	Annealing condition
Al-Mg-Pd RT-1/1	(a)	$Al_{50}Mg_{39.5}Pd_{10.5}$		104±13	400 °C, 2h
	Ref. 20	$Al_{50}Mg_{36}Pd_{14}$	0.81±0.01	217±10	400 °C, 3h
Al-Mg-Pd RT-QC	(b)	$Al_{42}Mg_{44}Pd_{14}$		190±10	400 °C, 2h
	Ref. 20	$Al_{42}Mg_{44}Pd_{14}$	0.62±0.01	221	400 °C, 3h
		$Al_{43}Mg_{44}Pd_{13}$		148±8	
		$Al_{44}Mg_{44}Pd_{12}$		143±10	
		$Al_{45}Mg_{44}Pd_{11}$		103±15	
Al-Mg-Pd MI-QC	(c)	$Al_{52}Mg_{17.5}Pd_{30.5}$		836±78	295 °C, 0h
	Ref. 10	$Al_{52}Mg_{18}Pd_{30}$	0.43±0.02	700±35	295 °C, 0h
Al-Mg-Zn RT-QC	Ref. 14	$Al_{15}Mg_{44}Zn_{41}$	0.77±0.01	120±12	300 °C, 2h
Al-Mg-Zn RT-1/1	Ref. 14	$Al_{20}Mg_{39.5}Zn_{40.5}$	1.04±0.01	76±8	300 °C, 2h

Neutron diffraction measurement was carried out to determine the radial distribution function RDF(r) for these three compounds. In addition, we have determined almost unambiguously the atomic structure for the RT-1/1 by using the powdered x-ray Rietveld analysis, from which both total and partial RDF(r) can be derived. By making full use of the Rietveld-refined RDF(r) spectra, we successfully extracted the structural difference between the RT-QC's and MI-QC's. The electronic structure, particularly the hybridization effect among various atomic pairs, is determined from a combination of the XPS and SXES, and the results are discussed in relation to the local atomic structures and the electron transport properties.

II. EXPERIMENTAL PROCEDURES

Alloy ingots were prepared with appropriate amounts of pure elements Al (purity $5N$), Mg ($4N$), and Pd ($4N$). The Al and Pd were firstly alloyed by arc melting. Here the addition of Mg was intentionally avoided, since Mg evaporates due to the excessive heating during the exothermic reaction between Al and Pd. Then the Al-Pd alloy ingot thus obtained was inductively alloyed with pure Mg in a graphite crucible under a pressurized He gas atmosphere.

Thermodynamically stable $Al_{42}Mg_{44}Pd_{14}$ RT-QC and $Al_{50}Mg_{39.5}Pd_{10.5}$ RT-1/1 were produced by melt spinning with subsequent annealing to enhance their structural quality. Metastable RT-QC and an amorphous phase were also obtained by melt spinning for $Al_{56-x}Mg_{44}Pd_x$ ($x=11$, 12, and 13) and $Al_{52}Mg_{17.5}Pd_{30.5}$, respectively.[9] The latter was transformed into the metastable MI-QC after the heat treatment. The structure of the as-quenched and annealed samples was examined by the x-ray diffraction with Cu K_α radiation. Dark-field electron microscopy measurements and electron diffraction measurements were carried out with JEOL2010 at 200 kV. Numerical data of the compositions, the conditions of heat treatments, and the electronic properties obtained are summarized in Table I. The experimental data of Al-Mg-Zn RT-compounds previously reported are also listed as reference.[14]

The neutron diffraction measurements have been made for the RT-QC, the RT-1/1, and the MI-QC by using the total scattering spectrometer (HIT) installed in Booster Synchrotron Facility of KEK in Japan. Each structure factor $S(Q)$ was converted to RDF(r) by the Fourier transformation. Powdered x-ray step-scanned diffraction data were taken with a RIGAKU-RAD2 Bragg-Brentano diffractometer with a curved PG diffracted beam monochromator, a 0.5° divergence slit, a 0.6 mm receiving slit, and a 0.5° scatter slit. This measurement was carried out only for the RT-1/1 with Cu K_α radiation and a 1 Hz rotating sample holder in the range from $2\theta=13°$ to 100°. The crystal structure of the RT-1/1 was determined by analyzing the powdered x-ray diffraction data with the Rietveld refinement program, RIETAN.[15] Structural data thus obtained were converted to the RDF(r).

The XPS valence band spectra were measured at room temperature by using an Al K_α monochromated x-ray source with the energy of 1487 eV (Surface Science Instrument, X-probe). The SXES spectra of Al K_β (Al-3p distribution) and Mg K_β (Mg-3p distribution) were measured using an electron beam accelerated to 15 keV. The Fermi energy in the SXES spectra was determined by measuring the binding energy of the XPS Al-$2p_{3/2}$ core level and Al K_α (from $2p_{3/2}$ to $1s$) SXES line. The electrical resistivity was measured at 300 K for a series of $Al_{56-x}Mg_{44}Pd_x$ ($x=11$, 12, 13, and 14) RT-QC's. More details were described elsewhere.[10]

III. RESULTS AND DISCUSSION

A. Determination of the atomic structure

Figure 1 shows the powdered x-ray diffraction spectra measured with Cu K_α radiation for the Al-Mg-Pd RT-QC, RT-1/1, and MI-QC compounds. All diffraction lines can be decisively indexed in terms of the respective compounds. According to the higher-dimensional projection method,[16] the structure of the approximant is closely related to that of the corresponding QC. As can be seen from Fig. 1, each peak of the approximant arises from the splitting of the peak of the corresponding QC. The grain size of each sample was calculated from the full width at half maximum (FWHM) of the diffraction peaks by using the Scherrer equation. The thermodynamically stable RT-1/1 and RT-QC have grains of about 800 Å in diameter. On the other hand, metastable

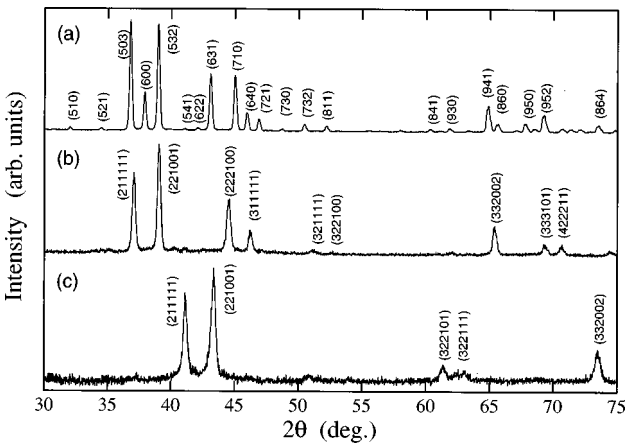

FIG. 1. X-ray diffraction spectra of (a) the $Al_{50}Mg_{39.5}Pd_{10.5}$ RT-1/1, (b) the $Al_{42}Mg_{44}Pd_{14}$ RT-QC, and (c) the $Al_{52}Mg_{17.5}Pd_{30.5}$ MI-QC.

MI-QC consists of grains which size is a few hundred angstrom in diameter. This can be confirmed easily in the electron microscopy image shown in Fig. 2. The $S(Q)$ spectra derived from the neutron diffraction experiment and the corresponding RDF(r) for the three compounds are shown in Figs. 3(A) and 3(B), respectively. Both $S(Q)$ and RDF(r) of the RT-QC are quite similar to those of the RT-1/1. In contrast, the spectrum of the MI-QC is obviously different from those of the RT compounds, indicating that the MI-QC possesses the atomic structure quite different from those of the RT compounds.

The RDF(r) spectra in the range up to 4 Å are blown up in Fig. 4. It is clear from Fig. 4 that the number of atomic pairs in the atomic distances up to 2.8 Å is obviously larger in the MI-QC than those in the two RT compounds. Note that the Goldschmidt radii of Al (1.43 Å) and Pd (1.37 Å) are

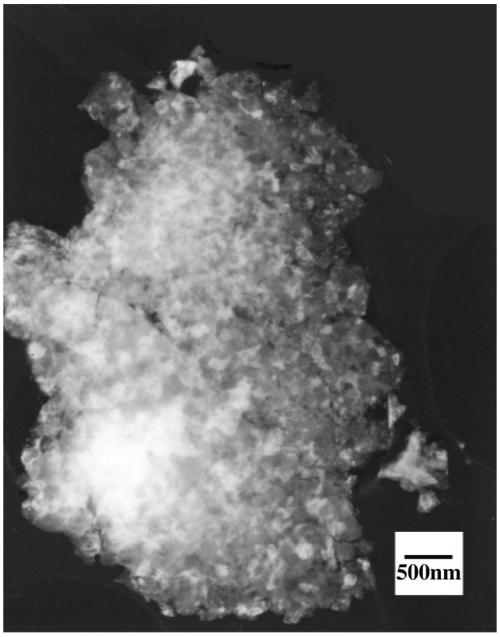

FIG. 2. Dark-field electron microscopy image for the $Al_{52}Mg_{17.5}Pd_{30.5}$ MI-QC. The large grain consists of small particles, the size of which is a few hundred Å in diameter.

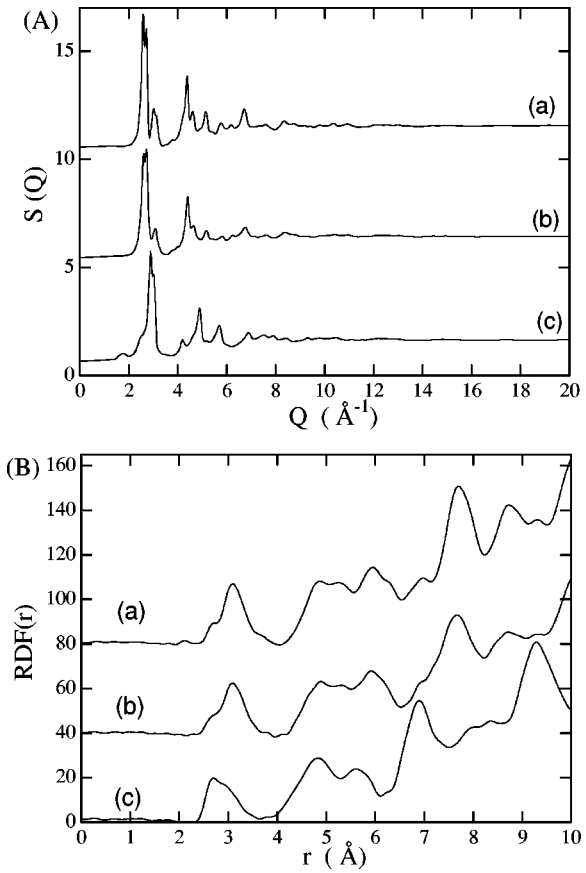

FIG. 3. (A) Structure factors $S(Q)$ and (B) the corresponding radial distribution functions RDF(r) for (a) the $Al_{50}Mg_{39.5}Pd_{10.5}$ RT-1/1, (b) $Al_{42}Mg_{44}Pd_{14}$ RT-QC, and (c) the $Al_{52}Mg_{17.5}Pd_{30.5}$ MI-QC derived from the neutron diffraction experiments.

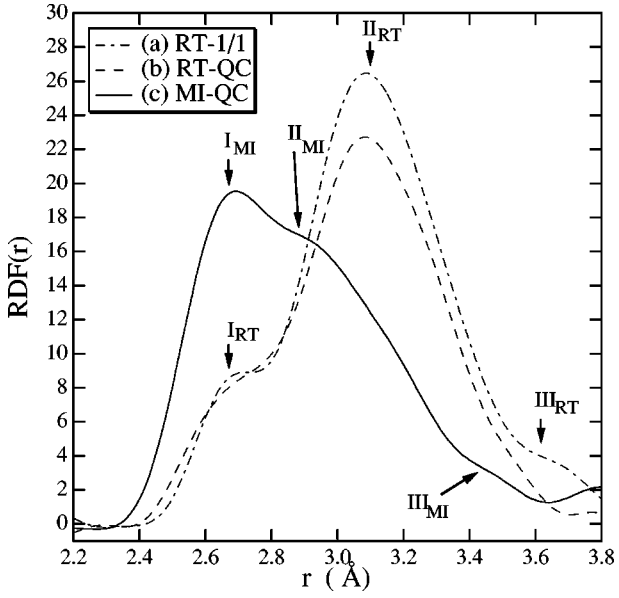

FIG. 4. Radial distribution functions RDF(r) for (a) the $Al_{50}Mg_{39.5}Pd_{10.5}$ RT-1/1, (b) the $Al_{42}Mg_{44}Pd_{14}$ RT-QC, and (c) the $Al_{52}Mg_{17.5}Pd_{30.5}$ MI-QC derived from the neutron diffraction experiments. Arrows indicating the first, second, and third peaks in each spectrum are due to the (Al, Pd)-(Al, Pd), (Al, Pd)-Mg, and Mg-Mg atomic pairs, respectively.

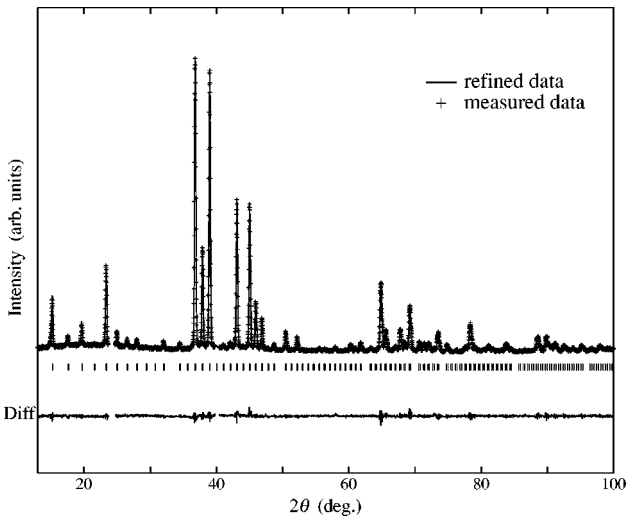

FIG. 5. X-ray diffraction data and refined spectrum fitted with the Rietveld program for the $Al_{50}Mg_{39.5}Pd_{10.5}$ RT-1/1. Bars indicate the allowed peak positions, and diff. shown at the bottom indicates the differences between the measured and the fitted data.

about 10% smaller than that of Mg (1.60 Å) and that the concentration of smaller atoms Al and Pd in the MI-QC amounts to 79–83 at. % whereas that in the RT compounds to only 54–64 at. %.[10,17] All this evidence leads us to conclude that the RDF(r) in the range up to about 2.6 Å in all three compounds is almost exclusively composed of the smaller atoms Al and Pd, and that the difference in the RDF(r) between the MI-QC and the RT compounds reflects that in the number and distribution of smaller atoms Al and Pd.

More important to be noted is the difference in the shortest range near 2.4 Å. A very edge of the first peak in the MI-QC is located at a distance much shorter than those in the RT compounds. Furthermore, a subtle but finite difference can be seen in the very edge of the spectra between the two RT-compounds; that of the RT-QC is more extended toward a shorter distance than that of the RT-1/1. We consider the difference in the very edge position among the three compounds to be very crucial and will focus on its details later.

Before analyzing the RDF(r) spectra, we must discuss, at this stage, the atomic structure of the RT-1/1 determined by the Rietveld refinement. Mizutani *et al.*[18] recently reported that the atomic structure for a series of $Al_xMg_{40}Zn_{60-x}$ RT-1/1 compounds has been successfully determined by analyzing the powdered x-ray diffraction spectra with the Rietveld refinement program. Here the refinement is carried out by using the model by Bergman, Waugh, and Pauling[19] as a starting structure. According to Bergman, Waugh, and Pauling,[19] four atomic sites denoted as D, E, G, and H are exclusively occupied by Mg atoms, and the smaller atoms Al and Zn are randomly distributed at certain ratios over the remaining atomic sites. In the present work, we employed the same approach as employed by Mizutani *et al.*[18] to determine the atomic structure of the Al-Mg-Pd RT-1/1. As shown in Fig. 5, the diffraction spectrum after the Rietveld refinement agrees very well with the observed one. The relevant numerical data are listed in Table II. The R_{wp}, R_I, and S which are taken as measures for the precision of the fitting,[15] are reduced to 6.95, 2.66, and 1.45%, respectively. Judging from the resulting R factors and the overall agreement between the refined and observed diffraction spectra, we conclude that the atomic structure of the Al-Mg-Pd RT-1/1 is decisively determined by the present Rietveld refinement.

As noted above, all Mg atoms are filled in the atomic sites D, E, G, and H without vacancies. An excellent refinement achieved in the present Rietveld analysis has confirmed the validity of this assumption. On the other hand, the Al and Pd atoms are randomly distributed at a given ratio over given atomic sites, as listed in Table II. This means that the absolute position of individual Al and Pd atoms cannot be uniquely determined and that the chemical disorder inherently exists in the distribution of Al and Pd atoms in the RT-1/1. This must be responsible for the relatively large residual resistivity observed in the RT-1/1 compounds,[14,20,21] even though the width of the x-ray diffraction peaks are fairly sharp.

TABLE II. Starting and final structural parameters.

$Al_{50}Mg_{39.5}Pd_{10.5}$ [$R_{wp}=6.95\%$, $R_I=2.66\%$, $R_F=2.06\%$, $R_e=4.78\%$, $S=1.45$ space group $Im\bar{3}$, $a=14.245(2)$ Å]											
	Atoms		Starting parameters				Refined data				
Site	Kind	WYCKNOT.	X	Y	Z	occ.	X	Y	Z	B_{iso}	occ.
A	Al	2(a)	0.00	0.00	0.00	0.80	0.0000	0.0000	0.0000		0.00
B	Al	24(g)	0.00	0.09	0.15	0.83	0.0000	0.0920(3)	0.1546(2)	0.41(3)	0.73
	Pd					0.17				0.41(3)	0.27
C	Al	24(g)	0.00	0.17	0.30	0.83	0.0000	0.1781(2)	0.3093(3)	0.41(3)	0.92
	Pd					0.17				0.41(3)	0.08
D	Mg	16(f)	0.18	0.18	0.18	1.00	0.1869(3)	0.1869(3)	0.1869(3)	1.2(2)	1.00
E	Mg	24(g)	0.00	0.20	0.11	1.00	0.0000	0.3009(3)	0.1205(4)	1.0(2)	1.00
F	Al	48(h)	0.16	0.18	0.41	0.83	0.1579(2)	0.1878(1)	0.4039(1)	0.41(3)	0.80
	Pd					0.17				0.41(3)	0.20
G	Mg	12(e)	0.40	0.00	0.50	1.00	0.4046(5)	0.000	0.5000	0.5(2)	1.00
H	Mg	12(e)	0.18	0.00	0.50	1.00	0.2009(5)	0.000	0.5000	0.7(2)	1.00

As one of the most characteristic features found in the present Rietveld analysis, we point to the absence of the center atom in the icosahedron of the first shell. Bergman, Waugh, and Pauling[19] originally reported that the atomic site A corresponding to the center of the icosahedron in the first shell is 80% occupied by the Al atom in the Al-Mg-Zn RT-1/1. However, the Rietveld analysis for a series of the $Al_xMg_{40}Zn_{60-x}$ RT-1/1 ($20 \leqslant x \leqslant 50$) compounds mentioned above showed that the occupancy of the site A is less than 20% in the range $20 \leqslant x < 30$, but that it is essentially vacant in the range $30 \leqslant x \leqslant 50$.[18] Similarly, the absence of the center atom has been reported in the structural analysis for the Al-Li-Cu RT-1/1 approximant.[22,23] Therefore, we believe that the center site A of the RT-1/1 compounds including the present Al-Mg-Pd RT-1/1 is vacant and that the RT-1/1 compounds contain 160 atoms rather than 162 atoms in the unit cell.

To extract more quantitative information from the Rietveld analysis, we normalize the interatomic distance with respect to that evaluated from the sum of the Goldschmidt radii for the corresponding atomic pairs:

$$r^{M-N}_{normalized} = \frac{r^{M-N}_{Rietveld}}{r^{M-N}_{Goldschmidt}} = \frac{r^{(M-N)}_{Rietveld}}{(C^M_{Al} r_{Al} + C^M_{Pd} r_{Pd}) + (C^N_{Al} r_{Al} + C^N_{Pd} r_{Pd})}, \quad (1)$$

where r^{M-N} is the interatomic distance between the sites M and N. C^N_X is the occupancy of the atom X at the site N and r_X is the Goldschmidt radius of the atom X. The normalized interatomic distances thus obtained are summarized in Table III. It is clear that the normalized interatomic distances of the (Al, Pd)-(Al, Pd) atomic pairs are always lower than unity, indicating the reduction in the interatomic distances relative to the hard sphere packing. In contrast, those for the Mg-(Al, Pd) atomic pairs marked with the asterisk in Table III are always close to unity. This implies that a large number of Al-Pd pairs possess reduced atomic distances but essentially no shortened Mg-Pd pairs in the structure of the RT-1/1 compound.

Now we are ready to construct the RDF(r) spectra from the Rietveld refined atomic structure for the RT-1/1. Here the delta functionlike pair distribution derived from the Rietveld analysis is multiplied by an appropriate Gaussian distribution function and coherent scattering length to allow a direct comparison with the measured $RDF^N(r)$ derived from the neutron diffraction experiment. As shown in Fig. 6(A), the resulting $RDF^R(r)$ can reproduce well the $RDF^N(r)$.

The partial radial distribution functions $RDF^R_{X-Y}(r)$ associated with the atomic pair X-Y in the RT-1/1 can be similarly constructed from the refined atomic structure. Three different $RDF^R_{X-Y}(r)$ spectra for the (Al, Pd)-(Al, Pd), Mg-(Al, Pd), and Mg-Mg atomic pairs are shown in Fig. 6(B), along with the $RDF^N(r)$ and the total $RDF^R(r)$. Note here that positions of the smaller atoms Al and Pd cannot be distinguished from one another so that they are shown in the bracket. We can see in Fig. 6(b) that the total RDF(r) in the distances up to 4 Å is made up of three peaks, as marked by arrows (I), (II), and (III), and that they are identified as mainly arising from the (Al, Pd)-(Al, Pd), (Al, Pd)-Mg, and Mg-Mg atomic pairs, respectively.

TABLE III. Interatomic distances derived from the refined crystalline structure for the $Al_{50}Mg_{39.5}Pd_{10.5}$ RT-1/1. The data with asterisks refer to the normalized interatomic distances associated with Mg-Pd pairs.

Atomic site		$Al_{50}Mg_{39.5}Zn_{10.5}$ $r^{M-N}_{Rietveld}$	$r^{M-N}_{renormalized}$
A	*B*	2.562	
B	*B*	2.622	0.93
		2.713	0.96
	C	3.520	0.89
	D	3.020	**1.00***
	E	3.003	**1.00***
		3.014	**1.00***
C	*D*	3.183	**1.05***
	E	3.066	**1.01***
		3.205	**1.06***
	F	2.711	0.95
		2.624	0.92
	G	2.962	**0.98***
	H	3.221	**1.06***
C	*D*	3.116	0.97
	E	3.258	1.02
	F	3.119	**1.03***
		3.123	**1.03***
E	*E*	3.437	1.07
	F	3.097	**1.03***
		3.109	**1.03***
	G	3.585	**1.12***
	H	3.056	0.96
F	*F*	2.704	0.95
		2.704	0.97
	G	2.941	**0.97***
	H	3.068	**1.02***
		3.074	**1.02***
G	*G*	2.724	0.85
	H	2.903	0.91
		3.166	0.99

The decomposition of the total RDF(r) into their partials for both RT-QC and MI-QC shown in Fig. 4 may be also made possible by making full use of the partial RDF(r) of the RT-1/1 as a guide. As mentioned above, the very edge of the first peak in the MI-QC extends to the shortest distance among these three compounds. We can also see that the intensity of RDF(r) in the region up to 2.6 Å in the MI-QC is twice as large as that in the RT compounds. These results strongly indicate that the extremely shortened (Al, Pd)-(Al, Pd) pairs do exist in the MI-QC structure. The second peak

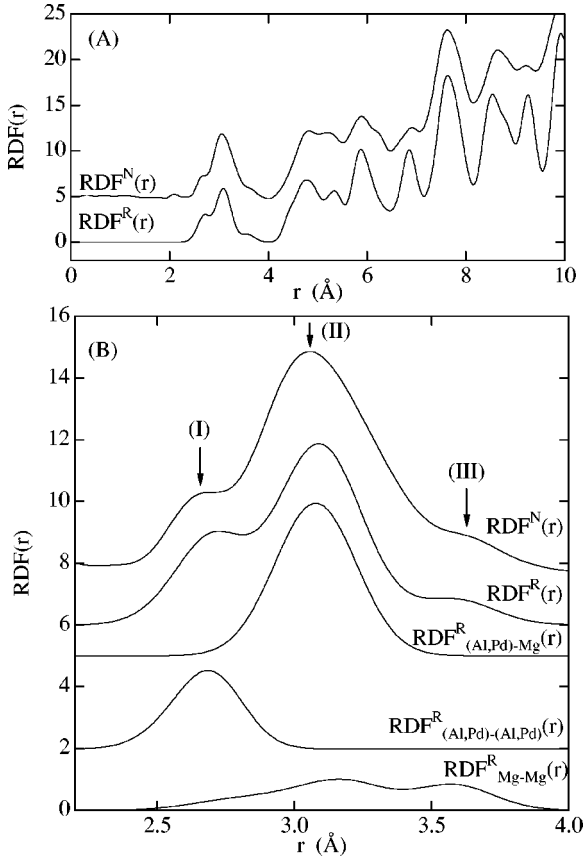

FIG. 6. (A) Total radial distribution function $\mathrm{RDF}^N(r)$ derived from the neutron diffraction experiments and total radial distribution function calculated from the refined crystal structure $\mathrm{RDF}^R(r)$ for the $Al_{50}Mg_{39.5}Pd_{10.5}$ RT-1/1. (B) Calculated partial radial distribution functions $\mathrm{RDF}^R_{(Al,\,Pd)-Mg}(r)$, $\mathrm{RDF}^R_{(Al,\,Pd)-(Al,\,Pd)}(r)$, and $\mathrm{RDF}^R_{Mg-Mg}(r)$ with $\mathrm{RDF}^R(r)$ and $\mathrm{RDF}^N(r)$ at the range from 2.2 to 4.0 Å.

marked as II_{MI} is observed at about 2.9 Å in the RDF(r) of the MI-QC, as shown in Fig. 4. We can attribute this to the contribution from the (Al, Pd)-Mg pairs. If this is correct, then we realize its position to be shifted to a shorter distance than that of the RT compounds (see the peak at 3.1 Å marked as II_{RT}). This means that the MI-QC is characterized by the possession of very shortened (Al, Pd)-(Al, Pd) pairs and also (Al, Pd)-Mg pairs relative to those in the RT compounds. This conclusion must be strengthened by other experimental evidences, which will be provided by the XSP and SXES studies in the next section.

Before ending this section, it is worthwhile mentioning that the very edge of the RDF(r) of the RT-QC is located at a distance slightly shorter than that of the RT-1/1. This can be taken as a signal that the interatomic distance of the (Al, Pd)-(Al, Pd) pairs in the RT-QC is more shortened than that in the RT-1/1. However, this should not be regarded as features characteristic of the local atomic structures of the RT-QC and RT-1/1. This is because the local atomic structure of these two compounds must be essentially identical when compared at a given composition. Instead, the difference in the edge structure between the RT-QC and RT-1/1 simply reflects the different Pd concentrations in the respective samples (10.5 at. % Pd in the RT-1/1 whereas 14 at. % Pd in the RT-QC).

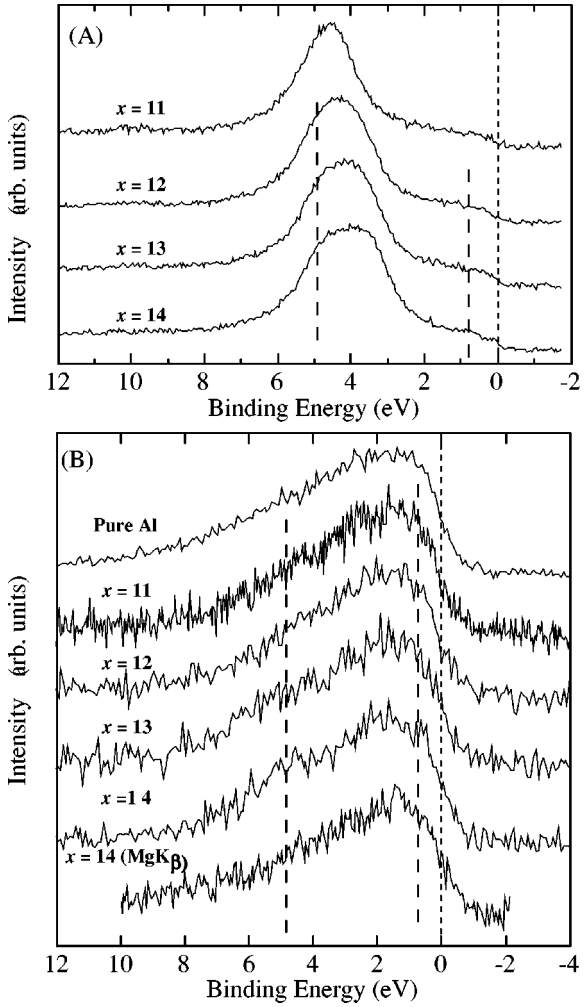

FIG. 7. (A) XPS and (B) Al K_β SXES spectra for the series of the $Al_{56-x}Mg_{44}Pd_x$ RT-QCs ($x=11$, 12, 13, and 14). Mg K_β SXES spectrum for $x=14$ is also shown at the bottom. The large peak near 4 eV on the XPS spectrum is due to the Pd-4d band.

B. Interrelationship between the local atomic structure and electronic structure

In this section, we discuss the inter-relationship between the local atomic structure and the electronic structure of the three relevant compounds in the Al-Mg-Pd system and gain further deeper insight into the mechanism for the possession of a higher resistivity in the MI-QC than that in the RT compounds.

1. RT compounds

Figure 7(a) shows the XPS valence band spectra for the $Al_{56-x}Mg_{44}Pd_x$ ($x=11$, 12, 13, and 14) RT-QC's. A large peak observed at about 3–4 eV for each spectrum can be safely ascribed to the Pd-4d states because of its large photoionization cross section. The width of the Pd-4d band for the $x=11$ sample is quite narrow, thereby indicating that the tail of the Pd-4d band hardly extends to E_F. Hence, the electronic structure of the RT-QC with $x=11$ is quite similar to that of noble metals. With increasing Pd concentration, however, one can clearly see an increase in the width of the Pd-4d band together with the displacement of its peak toward lower binding energies (BE). Therefore, the effect of

the Pd-4d states on the electronic states at the Fermi level definitely increases as increasing the Pd concentration within the stable concentration range of the RT-QC. It must be also noted that small humps grow at the BE of about 1 and 5 eV with increasing the Pd concentration in the RT-QC. These humps most likely represent the Pd-4d states perturbed by the hybridization with the surrounding atoms. The measurement of the SXES spectrum is very powerful to identify the electronic states hybridized with the Pd-4d states.

The Al K_β SXES spectra are known to reflect the Al-3p electron distribution.[10] The spectra of the RT-QC's are shown in Fig. 7(b) along with that of pure Al. The spectrum of the $x=11$ sample is quite similar to the pure Al spectrum without any indication of the formation of the bonding states. This is consistent with the corresponding XPS spectrum in Fig. 7(a). With increasing Pd concentration, however, weak but measurable humps grow at BE$=1$ and 5 eV. The energies of these humps in the Al K_β spectra agree well with the humps in the XPS spectra mentioned above. The Mg K_β SXES spectrum is incorporated in Fig. 7(b) for the RT-QC with the maximum Pd concentration $x=14$. This reflects the Mg-3p electron distribution. Obviously, the spectrum is fairly smooth without any measurable humps. Summarizing these results, we reach the conclusion that the humps at BE $=1$ and 5 eV are definitely caused by the hybridization between the Pd-4d and the Al-3p states and that the hybridization between the Pd-4d and Mg-3p states is insignificant in the RT-QC.

The gradual growth of the Al-Pd bonding states observed in the XPS and SXES spectra in the RT-QC must be reflected in the Pd concentration dependence of the interatomic distance of the Al-Pd atomic pairs in the RT-QC. Hence, let us direct our attention once again to the RDF(r) spectra shown in Fig. 4(b). As mentioned in the preceding section, the Pd concentration of the RT-QC is 14 at. % whereas that of the RT-1/1 is 10.5 at. %. Indeed, they represent the maximum and minimum Pd concentrations in the RT compounds.[24] The very edge of the RT-QC's RDF(r) spectrum, which exclusively represents the distribution of (Al, Pd)-(Al, Pd) atomic pairs, is located at a distance slightly shorter than that of the RT-1/1. As already mentioned, the local atomic structure of the RT-1/1 is essentially the same as that of the RT-QC at a given composition. The shift of the edge towards shorter distances must be brought about by an increase in the Pd concentration, since an increase in the Al-3p and Pd-4d hybridization effect contributes to shorten the interatomic distance of the Al-Pd atomic pair within the stable RT compounds. We have also noted in the preceding section that a substantial reduction in the interatomic distance is observed only in the Al-Pd pairs but not in the Mg-Pd pairs in both the RT-QC and the RT-1/1. This is also consistent with the XPS and SXES spectra discussed above.

We have shown above that the hybridization effect between Al-3p and Pd-4d states in the present Al-Mg-Pd RT-QC increases with increasing the Pd concentration. The electronic states near E_F are increasingly affected with increasing the Pd content and, hence, its effect would be reflected in the Pd concentration dependence of the electrical resistivity. Figure 8 shows the Pd concentration dependence of the resistivities at 300 K for a series of the $Al_{56-x}Mg_{44}Pd_x$ RT-QC's. Indeed, the resistivity rapidly increases with increasing Pd concentration. This is consistent with the present interpretation.

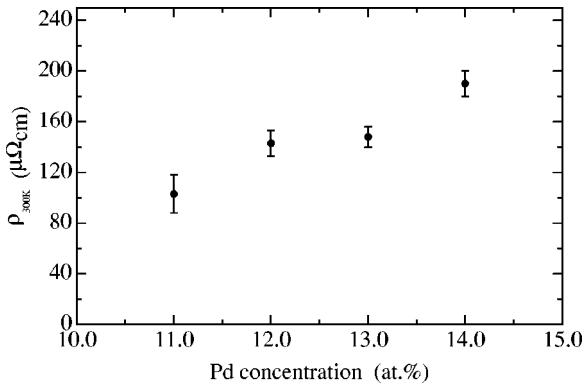

FIG. 8. Composition dependence of the resistivity at room temperature for the series of the $Al_{56-x}Mg_{44}Pd_x$ RT-QC.

Janot[25] pointed out that nearest-neighbor distances in the Al-Pd-Mn MI-QC have been found to be up to 5% shorter than in the corresponding metals. His interpretation on this reduction is that the intra-atomic transfer of electrons, for example from s to d in Pd, makes the size of atoms smaller. Indeed, the size reduction accompanied by the intra-atomic electron transfer can be effective.[26] Ionization caused by the interatomic electron transfer also would affect the atomic size. However, we found the strong evidence of the hybridization between Pd and simple metals in the valence band spectra, so that we believe that it is the overlap of the orbitals rather than the intra-atomic electron transfer or ionization to make the interatomic distances effectively shorter in the structures of the Al-Mg-Pd RT-QC and its approximants.

2. MI-QC

In sharp contrast to the RT compounds, the MI-QC is characterized by the possession of the shortened interatomic distance of both Al-Pd and Mg-Pd pairs. This may be taken as a clue to hint the role of Mg atom different from that in the RT compounds. As emphasized earlier, Mg atoms are filled at 100% proportion at the atomic sites denoted as D, E, G, and H in the RT-1/1 compound. Indeed, the Frank-Kasper phases, into which the RT-1/1 is classified, are composed of Kasper polyhedra that can be subdivided into tetrahedra having close packed atoms at each vertex without vacancies.[27] Hence, the size of atoms always plays an important role in the structure of the Frank-Kasper phases, and the Mg atom in the RT compounds acts as the role of a larger atom whereas Al and Pd atoms as that of smaller atoms to fill the space in a closed packed manner. This situation no longer holds in the MI-QC.

The MI-QC's are generally composed of 70–80 at. % Al and 30–20 at. % transition metals without involving Mg atoms. Provided that 20–30 at. % of transition metals is always needed in the construction of the MI-QC, all Pd atoms play this role in the MI-QC. On the other hand, Mg atoms expected to play the same role as that of Al to construct the MI-QC structure with the 20–30 at. % transition metal Pd. Since Mg atom can donate only s and p electrons to the valence band in the same manner as Al does. This strongly

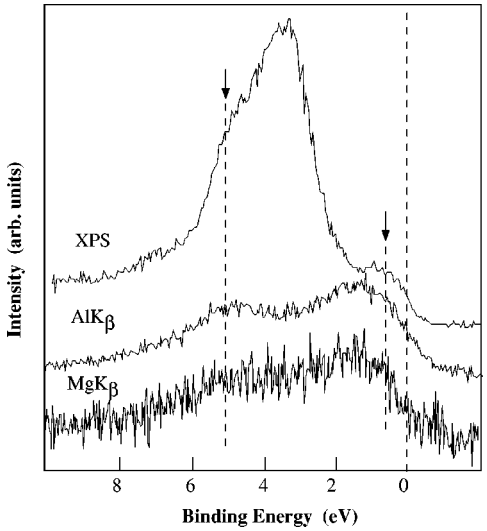

FIG. 9. XPS, Al K_β SXES, and Mg K_β SXES spectra of the $Al_{52}Mg_{17.5}Pd_{30.5}$ MI-QC. The position of bonding and the antibonding states is shown with vertical dashed lines.

supports that Mg atoms are most likely substituted for the sites of Al atoms rather than those of Pd atoms in the structure of the Al-Mg-Pd MI-QC. Thus, we believe that the atomic environment around Mg atom may be the same as that around Al, and that the reduction in the Mg-Pd interatomic distance in the MI-QC originates from hybridization of Mg-3p with the Pd-4d states, as discussed in the preceding section.

Now, we focus on the inter-relationship between the atomic and electronic structures of the MI-QC. The XPS, Al K_β, and Mg K_β SXES valence spectra of the MI-QC are shown in Fig. 9. One can see that the bonding and antibonding states are clearly formed as a result of the hybridization between Al-3p and Pd-4d states, and that the degree of the hybridization in the MI-QC is apparently more remarkable than that in the RT compounds. To a great surprise, the formation of the bonding and antibonding states is visible even in the Mg K_β spectra, in sharp contrast to its absence in the RT-QC. The hybridization effect between Al-3p and Pd-4d as well as the Mg-3p and Pd-4p states observed in both Al K_β and Mg K_β spectra would naturally result in the shortening of the interatomic distances of both the Al-Pd and Mg-Pd atomic pairs. This is exactly what we observed in the RDF(r) spectra shown in Fig. 4. A shortening of the interatomic distances in the Al-Pd pair in the MI-QC is evidenced from the RDF(r) spectrum in the region less than 2.6 Å, and the interatomic distance of the Mg-(Al, Pd) atomic pairs in the MI-QC is also substantially shortened relative to the hard sphere radii (2.97–3.03 Å) or the peak of the Mg-(Al, Pd) partial distribution function of the RT compounds, which is marked with a symbol II_{RT} at 3.1 Å in Fig. 4.

As indicated by broken lines in Fig. 9, the antibonding states are observed in the valance band spectra of the MI-QC at the BE immediately below E_F. This is caused by the hybridization of the Pd-4d states with both the Al-3p and the Mg-3p states. The conduction electrons near E_F in the MI-QC would enhance the tendency toward the localization due to the existence of these antibonding states. Hence we conclude that the formation of the antibonding state very close to E_F coupled with the formation of the pseudogap must be responsible for the occurrence of high resistivities reaching 800 $\mu\Omega$ cm in the MI-QC.

IV. CONCLUSION

We have investigated the local atomic structure of the Al-Mg-Pd RT-QC, the Al-Mg-Pd RT-1/1, and the Al-Mg-Pd MI-QC by using the RDF(r) spectra derived from both the neutron diffraction experiment and the x-ray Rietveld analysis. The RT-QC and the RT-1/1 compounds are characterized by the possession of reduced Al-Pd interatomic distances. In contrast, the MI-QC is characterized by the possession of shortened Al-Pd and Mg-Pd interatomic distances. These unique structural features of the RT-QC and the MI-QC are found to be consistent with the corresponding valence band structures and can explain why the MI-QC possesses the electrical resistivities much higher than those in the RT-QC.

ACKNOWLEDGMENTS

We would like to thank Professor Takeshi Matsuda for his help during the sample preparation, and one of the authors (T.T.) also acknowledges Dr. Yuh Yamada and Professor Juan Carlos Campuzano for their valuable comments in the course of this work. T.T. was financially supported by JSPS Research. The research was also supported in part by the Sasagawa Scientific Research Grant from The Japan Science Society.

[1] S. J. Poon, Adv. Phys. **41**, 303 (1988).

[2] R. Tamura, K. Kirihara, K. Kimura, and H. Ino, in *Proceedings of the 6th International Conference on Quasicrystals*, edited by S. Takeuchi and T. Fujiwara (World Scientific, Singapore, 1998), p. 631.

[3] T. Klein, C. Berger, G. Fourcaudot, J. C. Grieco, and J. C. Lasjaunias, J. Non-Cryst. Solids **153/154**, 312 (1993).

[4] F. S. Pierce, Q. Guo, and S. J. Poon, Phys. Rev. Lett. **73**, 2220 (1994).

[5] Y. Honda, K. Edagawa, A. Yoshikawa, T. Hashimoto, and S. Takeuchi, Jpn. J. Appl. Phys., Part 1 **33**, 4924 (1994).

[6] F. S. Pierce, P. A. Bancel, B. D. Biggs, Q. Guo, and S. J. Poon, Phys. Rev. B **47**, 5670 (1993).

[7] R. Tamura, K. Kirihara, K. Kimura, and H. Ino, in *Proceedings of the 5th International Conference on Quasicrystals*, edited by C. Janot and R. Mosseri (World Scientific, Singapore, 1995), p. 539.

[8] R. Haberkern and G. Frithc, in *Proceedings of the 5th International Conference on Quasicrystals* (Ref. 7), p. 460.

[9] S. Yamaguchi, T. Takeuchi, Y. Yamada, U. Mizutani, T. Nakashima, and T. Matsuda, in *Proceedings of the 5th International Conference on Quasicrystals* (Ref. 7), p. 548.

[10] U. Mizutani, Y. Yamada, T. Takeuchi, K. Hahsimoto, E. Belin, A. Sadoc, T. Yamauchi, and T. Matsuda, J. Phys.: Condens. Matter **6**, 7335 (1994).
[11] T. Takeuchi, Y. Yamada, and U. Mizutani, in *Proceedings of the 5th International Conference on Quasicrystals* (Ref. 7), p. 534.
[12] E. Beline *et al.*, J. Phys.: Condens. Matter **8**, 3513 (1996).
[13] M. Krajčí, M. Windisch, J. Hafner, and G. Kresse, Phys. Rev. B **51**, 17 355 (1995).
[14] T. Takeuchi and U. Mizutani, Phys. Rev. B **52**, 9300 (1995).
[15] F. Izumi, *The Rietveld Method*, edited by R. A. Young (Oxford University Press, Oxford, 1993), Chap. 13.
[16] C. L. Henly and V. Elser, Philos. Mag. B **53**, L59 (1986).
[17] N. Koshikawa, K. Edagawa, and S. Takeuchi, Mater. Trans., JIM **34**, 188 (1993).
[18] U. Mizutani, W. Iwakami, T. Takeuchi, M. Sakata, and M. Takata, Philos. Mag. Lett. **76**, 346 (1997).
[19] G. Bergman, J. L. T. Waugh, and L. Pauling, Acta Crystallogr. **10**, 254 (1957).
[20] K. Hashimoto, Y. Yamada, T. Yamauchi, T. Tanaka, T. Matsuda, and U. Mizutani, Mater. Sci. Eng., A **181/182**, 785 (1994).
[21] K. Kimura, H. Iwahashi, T. Hashimoto, S. Takeuchi, U. Mizutani, S. Ohashi, and G. Itoh, J. Phys. Soc. Jpn. **58**, 2472 (1989).
[22] M. Audier, J. Pannetier, M. Leblank, C. Janot, J. M. Lang, and B. Dubost, Physica B **153**, 136 (1988).
[23] C. A. Guryan, P. W. Stephens, A. I. Goldman, and F. W. Gayle, Phys. Rev. B **37**, 8495 (1988).
[24] T. Takeuchi, Y. Yamada, T. Fukunaga, and U. Mizutani, Mater. Sci. Eng., A **181/182**, 828 (1994).
[25] C. Janot, J. Phys.: Condens. Matter **9**, 1493 (1997).
[26] L. J. Parker, T. Atou, and J. V. Badding, Science **273**, 95 (1996).
[27] F. C. Frank and J. S. Kasper, Acta Crystallogr. **11**, 184 (1958); F. C. Frank and J. S. Kasper, *ibid.* **12**, 483 (1959).